Environmental Science & Technology

pubs.acs.org/est

Article

A Ventilated Three-Dimensional Artificial Lung System for Human Inhalation Exposure Studies

Haoxuan Chen, Airi Harui, Yu Feng, Liqiao Li, Saagar Patel, Jacob Schmidt, Michael D. Roth, and Yifang Zhu*

Cite This: https://doi.org/10.1021/acs.est.4c08315

Read Online

ACCESS | Metrics & More | Article Recommendations | Supporting Information

ABSTRACT: Traditional in vitro and in vivo models for inhalation toxicology studies often fail to replicate the anatomical and physiological conditions of the human lung. This limitation hinders our understanding of intrapulmonary exposures and their related health effects. To address this gap, we developed a ventilated artificial lung system that replicates human inhalation exposures in four key aspects: (1) facilitating continuous breathing with adjustable respiratory parameters; (2) distributing inhaled aerosols through transitional airflow fields in 3D-printed airway structures, which enables size-dependent particle deposition; (3) duplicating the warm and humid lung environment to promote inhaled aerosol dynamics, such as hygroscopic growth; and (4) supporting the cultivation of human airway epithelium for aerosol exposure and toxicological analyses. As a proof-of-concept application, we exposed human bronchial epithelial cells to electronic cigarette aerosols in the system. Our results show that electronic cigarette particles undergo significant hygroscopic growth within the artificial lung, leading to a 19% greater deposition dose compared to data collected at room temperature and relative humidity. Additionally, short-term exposure altered epithelial production of the chemokine Fractalkine in a nicotine-dependent manner, but no acute toxic effects were observed. This artificial lung system provides a more physiologically relevant in vitro model for studying inhalation exposures.

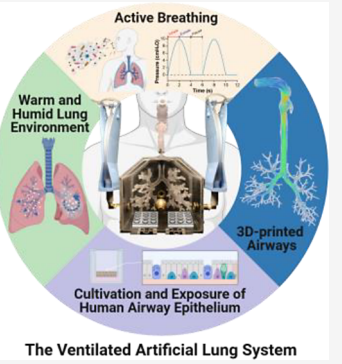

KEYWORDS: *artificial lung, inhalation toxicology, intrapulmonary exposure, airway epithelium, electronic cigarette*

1. INTRODUCTION

The human respiratory system functions as a crucial interface connecting the external environment to the systemic circulation. The respiratory epithelium is continuously exposed to an expanding array of airborne substances from various sources, including indoor and outdoor air pollution, tobacco smoke, electronic cigarettes (e-cig) aerosols, bioaerosols, microplastics, and engineered nanomaterials.[1−5] Exposure to harmful airborne substances substantially contributes to global morbidity and mortality resulting from associated respiratory and cardiovascular diseases.[6,7] For instance, according to the Global Burden of Disease study, air pollution [mainly particulate matter (PM)] and tobacco (including secondhand smoke) were associated with 8.08 million and 7.25 million premature deaths worldwide in 2021, respectively.[8,9] Therefore, it is of particular interest in environmental health studies to assess the inhalation exposure and subsequent health effects of various airborne substances. However, obtaining toxicology results that are representative of humans has been a longstanding challenge for both traditional in vivo and in vitro tests and new approach methodologies.[10,11] There is a need for new models that enhance our ability to better replicate and test inhalation exposures as they occur in real human lungs.

Knowing the characteristics of inhaled aerosols within human lungs is key to understanding exposure dose and related biological effects.[12] Inhaled particles deposit in the lungs through various mechanisms, including impaction (inertial force), sedimentation (gravity), Brownian diffusion, and interception.[13] These processes are influenced by particle size, airflow rate, and associated flow patterns (turbulent vs laminar), which vary across different lung sections.[14,15] Estimating particle inhalation exposure commonly involves using lung deposition models, such as the Human Respiratory Tract Model for Radiological Protection.[16] The lung deposition is predicted based on aerosol characteristics, such as particle size distributions and size-resolved toxic components, measured in the environment or under defined laboratory conditions.[17−22] However, experimental factors such as dilution ratio, temperature, and humidity substantially influence particle size distributions through aerosol dynamics, including coagulation, condensation, evaporation, and hygroscopic growth.[22,23] Consequently, it is uncertain whether aerosol characteristics measured under different conditions accurately represent those

Received: August 10, 2024
Revised: November 17, 2024
Accepted: November 27, 2024

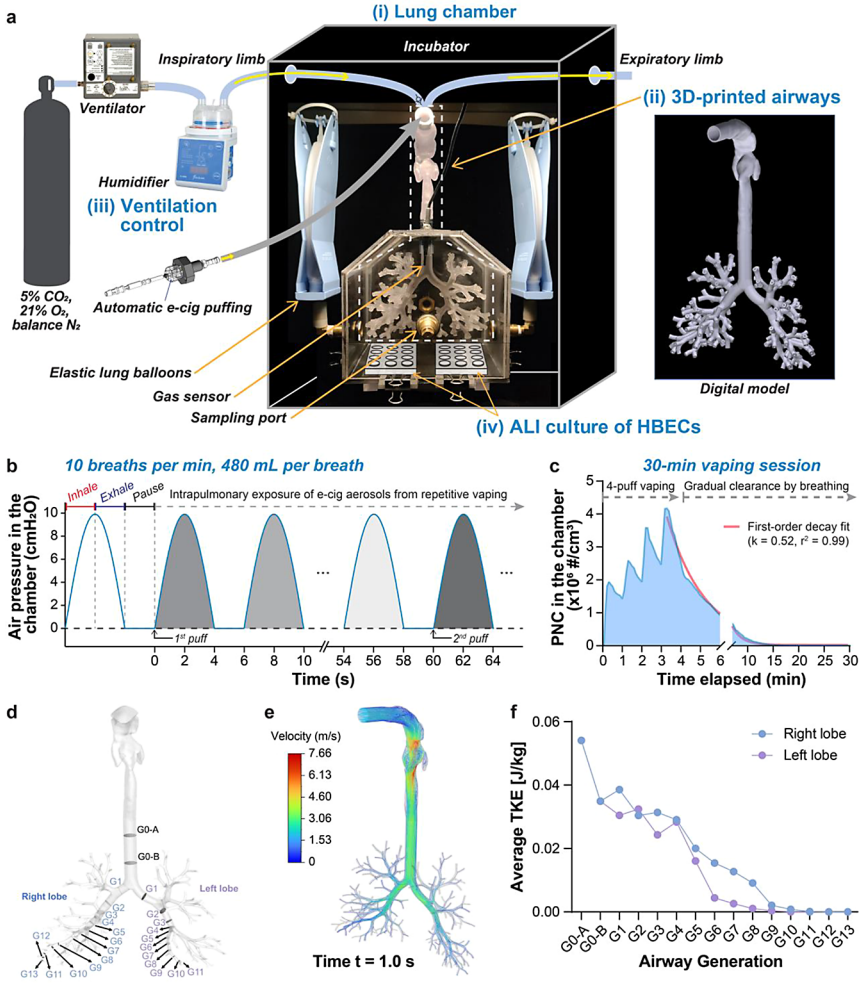

Figure 1. Ventilated artificial lung system. (a) Components of the ventilated artificial lung system: (i) lung chamber with temperature and humidity controlled by an incubator and humidifier; (ii) 3D-printed airway structures; (iii) ventilation control consisting of a ventilator with inspiratory and expiratory limbs and elastic lung balloons; and (iv) Air−liquid interface (ALI) culture of primary human bronchial epithelial cells (HBECs). (b) Illustration of the breathing cycles in integration with pulmonary exposure to e-cig aerosols from intermittent vaping. A typical 6-s breath cycle simulates breathing at rest for a normal person (10 BPM and 480 mL/breath): 2-s inhalation, 2-s exhalation, and 2-s pause, as employed in this study. For each vaping puff, 33 mL of e-cig aerosols were produced and introduced into the mouth inlet and then inhaled into the lungs during the following breath. The measured air pressure represents that within the artificial lung chamber above atmospheric pressure. (c) Real-time particle number concentrations (PNCs) in the lung chamber during a simulated 30 min vaping session, which includes 4-puff vaping (1 puff per minute) and the subsequent gradual clearance of particles by continuous breathing. The PNC curve after 4-puff vaping was fitted to a first-order decay. (d) Airway geometry used in this study for constructing the airway structures for 3D printing and computational fluid-particle dynamics (CFPD) simulation. Two representative routes of airflow in each lung lobe were labeled. (e) Streamlines colored by the airflow velocity magnitude in the airway structures at $t = 1$ s (1/2 inhalation) obtained from CFPD simulation. (f) Averaged turbulence kinetic energy (TKE) at different cross sections along two routes in each lung lobe.

in human lungs. Although recent progress has been made in computational inhalation toxicology assessment by integrating aerosol dynamic mechanisms and machine learning,[24−27] their predictive accuracy is limited by experimentally measurable parameters. Validation of modeling outcomes against experimental results is still necessary.[28] Recent studies have utilized in vitro human airway replicas created through three-dimensional (3D) printing to experimentally study the lung deposition of aerosols from different sources.[29−31] However, the dynamic respiratory processes and lung environment were not captured in those studies. To advance inhalation exposure assessment, new models are needed to better simulate the lung conditions and breathing patterns.

Experimental inhalation toxicology studies have heavily relied on animal models, which are different from humans in terms of respiratory physiology, exposure times, life cycles, and exposure conditions.[32−34] The difficulty in translating results from animals to humans, coupled with increasing ethical concerns regarding animal use, is driving the transition toward alternative approaches.[34] The development of organotypic air−liquid-interface (ALI) airway tissue derived from primary human airway progenitors has presented a unique opportunity to assess exposure and associated effects in vitro.[35−37] Recently, airway/alveolus-on-chip technology based on ALI was developed, and biomimetic engineering has enabled in vitro analysis of lung organoid pathophysiology and replication of inhalation exposure.[38−41] Despite these advancements, replicating the intricate respiratory process involving inhaled aerosol dynamics at the organ or system level remains challenging. For instance, the serial dilution and clearance of inhaled aerosols during continuous breathing result in dynamic exposure profiles over time. The key features of particulates linked to their toxicity

https://doi.org/10.1021/acs.est.4c08315
Environ. Sci. Technol. XXXX, XXX, XXX−XXX

potential, such as the chemical composition and oxidative potential, were shown to change significantly after entering the lung environment.[42] Furthermore, the lung's anatomy creates region-specific deposition patterns of inhaled particles.[14,43] These factors collectively limit our understanding of the toxicity associated with various inhalation exposures.

To address these challenges, we developed an artificial lung system as a more physiologically relevant in vitro model for human inhalation exposure. This system employs continuous breathing to distribute and deposit inhaled aerosols through 3D-printed airways. Computational fluid-particle dynamics (CFPD) modeling and experimental measurements using standard particles were conducted to test the system's ability to recreate regional airflow fields and associated size-dependent particle deposition in the 3D-printed airways. The system also replicates the human lung environment, including temperature, humidity, and gas compositions, facilitating aerosol dynamics similar to those in human lungs and supporting the cultivation of human primary airway epithelial cells. As a proof-of-concept application, we used the system to study e-cig aerosols, which possess unique volatility and hygroscopic properties of interest. The increasing popularity of e-cigs has led to serious public health concerns worldwide.[44,45] Current studies using traditional toxicology approaches often fall short in replicating the intrapulmonary exposure to e-cig aerosols, thus limiting our understanding of their respiratory health effects.[23,46,47] Utilizing the artificial lung system, we assessed the biological effects of e-cig aerosol exposure on human primary bronchial epithelium under simulated vaping scenarios.

2. MATERIALS AND METHODS

2.1. Development of the Artificial Lung System. As shown in Figure 1a, the developed artificial lung, enclosed within a temperature-controlled incubator, features a lung chamber that reproduces the size, shape, and volume of the average male human lung at end-inspiration (i.e., 6 L),[48] and a 3D-printed human airway structure including the upper airway (mouth to the trachea) and the branching tracheobronchial (TB) tree with the farthest distal airways at generation 13 (G13).

To enable the artificial lung to actively "breathe," a clinical-grade human ventilator was connected to the lung chamber incorporating elastic lung balloons on each side. The lung balloons expand during inhalation driven by the ventilator and then contract to "exhale" due to their elasticity, mimicking the volume changes of human lungs during breathing, as demonstrated in Video S1. Their combined compliance (0.048 L/cmH_2O) controls intrapulmonary pressure and flow dynamics during each breath, based on the respiratory parameters set on the ventilator. As such, the artificial lung can replicate different human breathing patterns with various respiratory rates [8−20 breaths per minute (BPM)], inspiratory times (1−2 s), and tidal volumes (200−1200 mL). In this study, a typical breathing pattern for a normal person at rest was set at 10 BPM and 480 mL/breath, generating a 6-s breath cycle composed of 2-s inhalation, 2-s exhalation, and 2-s pause before the next breath, as illustrated in Figure 1b.

A replica of human airways was prepared using high-resolution 3D printing (Form 3, Formlabs, Inc., USA) and installed in the lung chamber (Figure 1a). The airway geometry (Figure 1d) was developed by integrating an upper airway from computed tomography (CT) scans and a TB tree created using Lung4Cer based on a stochastic algorithm.[49,50] The model comprises 375 individual airway sections including 188 distal terminal airways. The farthest terminal airway printed in this model is the 13th branching generation (G13), with the smallest hydraulic diameter of 1.02 mm, best described as the level of preterminal bronchioles. At this generation, the fast turbulent airflow from the trachea transitions into slow laminar airflow,[51] before being distributed throughout the lung chamber. To assess airflow profiles and the transport of inhaled particles in the 3D-printed airway structures, we conducted computational fluid-particle dynamics (CFPD) simulations using the typical breathing pattern (10 BPM, 480 mL per breath) described above.

The temperature (37 °C) and relative humidity (RH, 88%) in the artificial lung chamber were independently controlled by a humidifier in the ventilatory limb and the incubator. The clinical blood gas mixtures (5% CO_2, 21% O_2, balance N_2) that replicate alveolar gas composition are used to ventilate the artificial lung. Therefore, the system replicates the heated, humidified, and CO_2-controlled environment similar to that of an incubator for airway cell cultures.

Detailed materials and methods for developing the artificial lung system and conducting CFPD simulations are provided in the Supporting Information.

2.2. Aerosol Generation and Experimental Conditions. In addition to e-cig aerosols, standard solid and liquid particles, sodium chloride (NaCl) and diethyl-hexyl sebacate (DEHS), were generated to test the developed artificial lung system. Two environmental conditions were created within the lung chamber: lung temperature and relative humidity [lung T/RH (37 °C/88%)] and room temperature and relative humidity [room T/RH (25 °C/38%)].

An e-cig puffing system was employed to generate e-cig aerosols using JUUL pods filled with different e-liquid formulations following programmed vaping patterns (Figure 1a).[52,53] In this study, we tested marketed Virginia Tobacco JUUL pods containing polyethylene glycol/vegetable glycerol (PG/VG) in a 30:70 ratio and 5% (w/w) nicotine benzoate. Additionally, we tested two lab-made e-liquid formulations that partially replicate the constituents of the Virginia Tobacco JUUL pods: one containing only PG/VG (30:70) and the other containing PG/VG (30:70) with 5% (w/w) nicotine benzoate.[53] A 33 mL puff of e-cig aerosols was delivered into the mouth inlet of the artificial lung during the 2-s pause and subsequently inhaled into the lung, which approximates the realistic vaping process that includes a puff and inhalation into the lung.[54] The particle number concentrations (PNCs) in the lung chamber were measured in real time using a nano water-based condensation particle counter (N-WCPC, Model 3788, TSI, Inc., USA). Dilution using compressed air at a ratio of 1:10 was applied to ensure that the PNCs were within the measurable range of the N-WCPC. The decay rates of particles under different breathing patterns were calculated (see Section 2.5 Data Analysis). The deposition of the e-cig particles in the artificial lung was characterized using a single-puff experiment conducted in the lung environment, in which the ventilator was immediately turned off after a puff of e-cig aerosols was delivered into the lung chamber. The size distributions of e-cig aerosols were measured using a Scanning Mobility Particle Sizer (SMPS, Model 3936, TSI, Inc., USA) and an Aerodynamic Particle Sizer (APS, Model 3321, TSI, Inc., USA). The measuring modes for the SMPS and APS were optimized and covered a size range of 13 to 445 nm for the SMPS (electric mobility diameter) and 542 nm to 20 μm for the APS (aerodynamic diameter); these ranges encompassed the majority of the particles emitted from e-cigs.

https://doi.org/10.1021/acs.est.4c08315
Environ. Sci. Technol. XXXX, XXX, XXX−XXX

DEHS and NaCl particles were generated using a condensation monodisperse aerosol generator (Model 3475, TSI, Inc., USA) and a collision nebulizer (CH Technologies Inc., USA), respectively. These particles were introduced into the artificial lung at a constant air flow rate equivalent to the adopted breathing pattern (i.e., 14.4 L min^{-1}). The schematic experimental setup and size-distributions of the generated DEHS and NaCl particles are provided in Figures S1 and S2, respectively. The size distributions of the particles were measured upstream and downstream of the artificial lung using the SMPS and APS. The calculation of deposition fractions is described in the Data Analysis section.

2.3. Predicted Lung Deposition of E-cig Particles. To investigate the impact of the lung environment on the deposition of e-cig particles, we employed the multiple-path particle dosimetry (MPPD) model (v 3.04) to estimate the deposition fractions and deposition doses throughout the entire human lung, including the upper airway (also referred to as the head airway in the MPPD model), TB airways, and alveoli.[55] The MPPD prediction adopted the stochastic airway geometry and the same breathing pattern as our experimental test (i.e., 10 breaths per min, tidal volume of 480 mL, and oral breath). The total and regional deposition fractions were estimated based on the observed bimodal size distributions of the e-cig aerosols. As discussed above, the increase in the mass of e-cig particles in the lung environment was attributed to water absorption by the e-cig particles from the surrounding environment. To estimate the deposition doses of the e-cig particles, we utilized the observed size characteristics for the two aerosol modes under the respective environmental conditions, while maintaining the same mass fractions for the two aerosol modes observed at room T/RH. The basic modeling parameters and detailed aerosol characteristics for the MPPD model prediction are tabulated in Tables S1 and S2, respectively.

2.4. Expose Human Bronchial Epithelial Cells to E-cig Aerosol. To match the simulated bronchiole exposure conditions in the artificial lung system, primary human bronchial epithelial cells (HBECs) were used in a proof-of-concept study to examine the toxic effects of e-cig aerosol exposures under physiologically relevant conditions. Primary HBECs closely mimic the native airway epithelium, maintaining key functions such as mucus production, mucociliary clearance, barrier integrity with tight junctions, and biological responses, thereby providing a more accurate representation of human respiratory biology than immortalized cell lines.[56] In this study, three independent replicate experiments using different batches of ALI cultures of HBECs from the same donor at the same passage were conducted on different dates. Detailed information on the materials and methods for HBEC cultivation is provided in the Supporting Information. Each experiment included four exposure groups: a control group (exposed to clean air) and three experimental groups exposed to e-cig aerosols produced from different e-liquids—PG/VG, PG/VG+Nic, and JUUL. These experimental groups are designed to recover major constituents of popular formulations, including the e-liquid base, nicotine salt, and other additives such as flavors, in a progressive manner.[57] The three experiments had sample sizes $n = 9$, 8, and 6 cell culture wells per group, respectively, totaling $n = 23$ for each group. On the day of exposure, fully differentiated HBEC layers in ALI cultures were placed in the lung chamber with (e-cig exposure groups) or without (control group) exposure to e-cig aerosols through simulated intermittent vaping sessions over 2 days. Photos of the experimental settings are shown in Figure S3. Based on a study surveying e-cig use patterns,[22] HBEC cultures were exposed to 13 vaping sessions in 6.5 h (one vaping session every 30 min) per day. For each vaping session, 4 consecutive puffs were applied at 1 min intervals (1 puff per min, with a 2-s puff duration and a 33 mL puff volume) (Figure 1b,c). As a result, the artificial lung with HBEC cultures "vaped" a total of 104 puffs over 2 days. During times outside of exposure periods, the HBEC cultures were returned to the incubator.

After exposure, the HBEC tissue cultures and supernatant were collected for histological and biomarker analysis, respectively. The HBEC tissue cultures were fixed in 4% paraformaldehyde, embedded in paraffin, and 4 μm sections were prepared and stained using hematoxylin and eosin (H&E) by the Translational Pathology Core Laboratory at UCLA. Nicotine in the supernatant, as a biomarker of exposure, was quantified using gas chromatography−mass spectrometry (GC−MS, 6890/5975, Agilent Technologies, Inc., USA) according to our established method.[58] The chemokine Fractalkine (CX3CL1), as a biomarker of biological effects, was quantified via ELISA assay (DCX310, R&D Systems, Inc., USA) following the manufacturer's instructions using a BioTek Synergy HT microplate reader (Agilent Technologies, Inc., USA).

2.5. Data Analysis. *2.5.1. Aerosol Data.* For each experimental condition, at least three independent tests were conducted. The size distribution data from the SMPS and APS were matched for the same test and averaged from independent tests for each experimental condition using Data Merge software (TSI, Inc., USA). The particle mobility diameter measured by the SMPS was converted to the aerodynamic diameter, and the mass-based particle size distributions were calculated from the directly measured number-based particle size distributions by the SMPS and APS, assuming spherical particles with the density of corresponding materials (Table S3). Summary statistics, including the geometric mean, geometric standard deviation, total number, and mass concentration, were calculated for each aerosol mode. The deposition of the tested particles in the airway structures was determined based on the size-resolved particle concentrations before and after passing through the airway structure replica.[31] A detailed description of the calculation of the particle decay rate due to ongoing breathing and particle deposition in the 3D-printed airways is provided in the Supporting Information. Additionally, the differences in the aerosol characteristics (i.e., size geometric mean, total number and mass concentration) and the predicted deposition fractions and deposition doses in different lung regions and environmental conditions were assessed using t tests.

2.5.2. Biomarker Data. Biomarker data were first cleaned for values below the lower limit of quantitation (LLoQ) and outliers using the ROUT method ($Q = 1\%$). The data exhibited a normal distribution with sample sizes of $n = 23$ for each group. For nicotine, differences between the PG/VG+Nic and JUUL groups were tested using a paired t test with matched samples according to experimental batch and well locations in the plate. Differences in Fractalkine levels among the four groups were tested using ANOVA, also with matched samples according to experimental batch and well locations in the plate.

The statistical analysis and visualization of the results were performed using Prism 9 software (GraphPad Software, Inc., USA).

https://doi.org/10.1021/acs.est.4c08315
Environ. Sci. Technol. XXXX, XXX, XXX−XXX

3. RESULTS AND DISCUSSION

3.1. Dynamic Airflow Patterns in the Ventilated Artificial Lung. To demonstrate the realistic inhalation exposure scheme facilitated by the active breathing of the artificial lung system, we created a simulated 30 min session of vaping e-cigs integrated with the normal breathing pattern (10 BPM, 480 mL per breath). This session involved taking 4 puffs at a rate of one puff per minute, followed by subsequent ventilation, as illustrated in Figure 1b,c. The intrapulmonary exposure to e-cig aerosols during the 30 min session was monitored by measuring PNCs through the sampling port in real time. An example measurement, shown in Figure 1c, depicts the 4-puff vaping cycle creating a stepwise increase in peak PNCs within the lung chamber, followed by a gradual clearance of inhaled e-cig aerosol in a first-order decay (k = 0.52, r^2 = 0.99) due to continuous breathing.

The 3D-printed airway structure, spanning from the mouth inlet to G13 small airways (Figure 1d) facilitates the distribution of inhaled airflow within the lung chamber. CFPD modeling revealed that the peak airflow velocity during inhalation (Time = 1 s in Figure 1b) gradually decreases from the upper to lower airways as the total cross-sectional areas increase (Figure 1e). The averaged turbulence kinetic energy (TKE) was calculated at different cross sections along two routes in each lung lobe (Figure 1d,f). The overall decreasing trend of TKE from the trachea to distal airways suggests that the turbulence in the trachea-to-G2 airway region gradually transitions to laminar flow as it passes through each subsequent generation of airways. The airflow streamline profiles in different airway sections throughout a complete breath cycle are provided in Figure S4. The comparison of airflow in the trachea and distal airways was also visualized by introducing a puff of e-cig aerosols into the lung chamber with and without human airway structures (Video S1). Consequently, the flow rate and pattern exhibit regional variations, impacting the regional distribution and deposition of inhaled particles.

3.2. Particle Deposition in the 3D-Printed Airways. To evaluate particle deposition in the 3D-printed airways, we used e-cig particles as well as standard DEHS and NaCl particles under the typical breathing pattern (10 BPM and 480 mL/breath) or equivalent airflow (Figure S1). A "U" shaped deposition curve was observed for the size range of 20−10,000 nm (Figure 2). For e-cig and NaCl particles, which are primarily nano- and submicron particles, the deposition fraction increased as particle diameter decreased. The experiment conducted with DEHS particles provided the deposition fraction for the micron-size range where the deposition fraction increased as particle diameter increased. To further elucidate particle transport within the airways, CFPD simulations were conducted for particles of four sizes (10, 100 nm, 1, and 10 μm). As shown in Figure S5, distinct distribution and deposition patterns were observed for particles of different sizes, influenced by various mechanical forces within the dynamic airflow fields. Ultrafine particles (10 nm) exhibited higher deposition, driven primarily by Brownian diffusion. Similarly, coarse particles (10 μm) showed substantial deposition due to a combination of inertial impaction and gravitational sedimentation. In contrast, particles of intermediate sizes (100 nm and 1 μm) exhibited lower deposition, as neither mechanism was particularly effective for these sizes.

The obtained size-resolved particle deposition fractions were then compared to results from the MPPD model for the upper and TB airways. The MPPD modeling incorporated a similar stochastic airway geometry and the same breathing pattern as used in our experiments. The observed deposition curve of different particles in the upper and TB airways resulted from the combined effects of these different mechanisms.[13] In general, our experimental data exhibited similar trends to those predicted by the MPPD model. However, differences between our results and modeling predictions were expected for various reasons. For instance, our artificial lung utilized an upper airway geometry obtained from a CT scan of a specific volunteer, producing an individual-specific particle deposition curve. In contrast, the MPPD model incorporates semiempirical estimations of particle deposition in human lungs across a population.[59] Lung physiology, including airway geometry, varies with demographic factors, such as age, sex, and ethnicity, as well as lung conditions, which can lead to distinct exposure conditions. Future studies could develop different airway replicas with specific characteristics related to lung diseases or different groups to provide information on individual susceptibility to inhalation exposure.

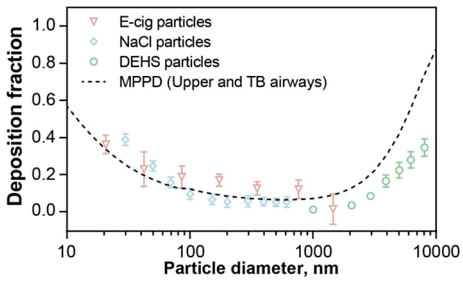

Figure 2. Size-resolved particle deposition fraction in the 3D-printed airway structures. The particle deposition was determined using e-cig, diethyl-hexyl sebacate (DEHS), and sodium chloride (NaCl) particles from at least three independent tests with error bars for the standard deviations. The solid line in the plot represents the modeled size-resolved particle deposition fraction in the upper and tracheobronchial (TB) tree via the multiple-path particle dosimetry (MPPD) model. The stochastic lung morphometry and the same breathing pattern (10 BPM, 480 mL tidal volume) as the experiments were used in the MPPD modeling to generate the deposition fraction curve.

3.3. Hygroscopic Growth of E-cig Particles in the Lung Environment. To demonstrate the effects of the warm and humid lung environment on particle properties, the size distributions of the e-cig particles were measured immediately after one puff was introduced into the lung chamber at room T/RH (25 °C/38%) and lung T/RH (37 °C/88%). A clear trimodal distribution of the e-cig particles under both conditions was observed (Figure 3a), with a primary mode at submicron sizes (300−400 nm), a secondary mode at ultrafine sizes (<100 nm), and a tertiary mode at micron sizes (1000−2000 nm). Note that the scales in Figure 3a are different for the two modes. The number concentrations of particles smaller than 500 nm were 3 orders of magnitude higher than those of particles larger than 500 nm, thus considerably contributing to the particle mass concentrations (Figure 3b). Due to the size gap between the measuring ranges of the SMPS and APS, the mass-based size distributions of e-cig aerosols did not form a continuous curve.

A warm and humid lung environment led to a significant increase in the geometric mean diameter of particles larger than 500 nm, from 1.32 (95% CI: 1.28−1.36) to 1.87 (95% CI: 1.58−2.16) μm (p < 0.01, t test) (Figure 3a,c). This was likely due to the hygroscopic growth of e-cig particles by absorbing water vapor in warm and humid lung environments. The hygroscopic growth of e-cig particles was also confirmed by the denser

https://doi.org/10.1021/acs.est.4c08315
Environ. Sci. Technol. XXXX, XXX, XXX−XXX

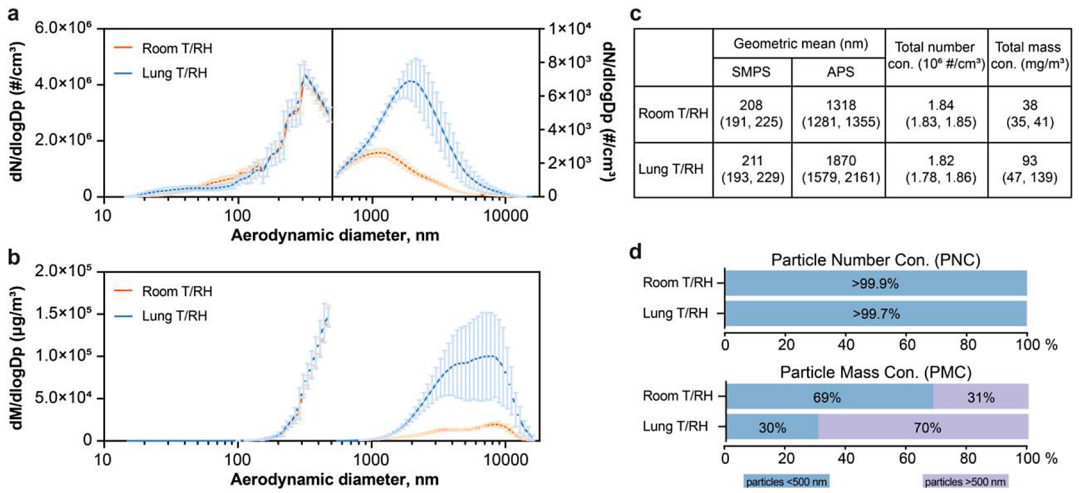

Figure 3. Particle size distribution of the e-cig aerosols in the artificial lung system. (a) Number-based and (b) mass-based particle size distribution of the e-cig aerosols in room and lung environmental conditions. (c) Summary data of the e-cig aerosols including the geometric means, total number concentrations, and total mass concentration. The data are presented with 95% confidence intervals. (d) Percentage contributions of different size regimes to the total particle number and mass concentrations. E-cig aerosols were classified as small particles (<500 nm, measured by a Scanning Mobility Particle Sizer) and large particles (>500 nm, measured by an Aerodynamic Particle Sizer).

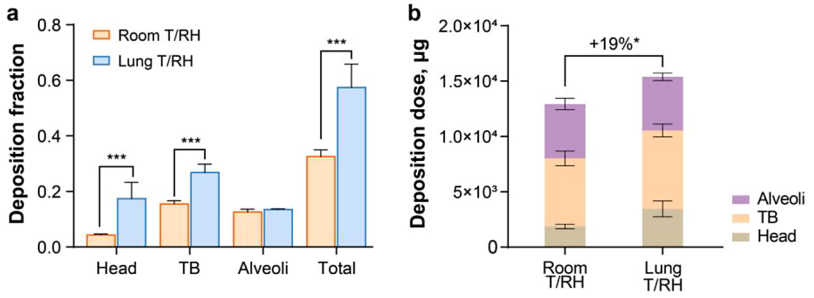

Figure 4. Impact of hygroscopic growth on e-cig particle deposition. (a) Deposition fraction and (b) deposition dose of e-cig aerosols in different lung regions under room T/RH (25 °C, 38% RH) and lung T/RH (37 °C, 88% RH), as predicted by the MPPD model. The stochastic lung morphometry and the same breathing pattern (10 BPM, 480 mL tidal volume) used in the experimental measurements were incorporated into the MPPD modeling.

"clouds" of e-cig aerosols that formed within the lung environment as demonstrated in Video S2. This also caused a significant increase in the total mass concentration by 2.4-fold (Figure 3c). Given that hygroscopic growth results in particles with slightly lower densities than the original e-cig particles, this estimation could be underestimated. Nevertheless, small particles accounted for the majority of the total number concentration in both the room T/RH (>99.9%) and the lung T/RH (>99.7%) (Figure 3d). However, large particles contributed more to the total mass concentration than small particles in the lung environment due to mass gain from hygroscopic growth. We did not observe any differences in the total number concentrations and size increase of the submicron particles between the two conditions.

According to the deposition fraction curve (Figure 2), the hygroscopic growth of e-cig particles in the lung environment is anticipated to lead to higher exposure doses. Additionally, the variations in airway structures and airflow characteristics across different lung sections may result in enhanced particle deposition with a region-specific pattern.[14] This is important for understanding the pathology of respiratory diseases associated with inhalation exposure.[60,61] To illustrate the comprehensive lung deposition profile of e-cig particles and the effects of the lung environment, we used the MPPD model to predict lung deposition based on the observed size distributions. Particle growth in the artificial lung was shown to cause over 70% more total deposition fractions compared to the room condition (Figure 4a). Enhanced deposition was observed predominantly in the upper and TB airways rather than in the alveolar regions, primarily due to the substantial growth of micron-sized particles. Overall, hygroscopic growth resulted in a mass gain of more than 140% for e-cig particles in the warm and humid lung environments. However, elevated deposition fractions do not necessarily reflect the deposition doses of e-cig components, as the increased mass is mainly attributed to water vapor. By applying the same mass fractions distributed for the two aerosol modes as observed at room T/RH in the MPPD model, we estimated that the increase in particle size in the lung environment led to a 19% greater deposition dose compared to the room condition (Figure 4b). These results emphasize the importance of considering hygroscopic growth in inhalation exposure assessments, particularly when using lung deposition models.

In addition to e-cig particles, various other airborne particles, such as cigarette smoke, aerosolized pharmaceuticals, and environmental aerosols from different sources, exhibit varying degrees of hygroscopicity. The hygroscopic growth factor (HGF) of these particles, as reported in previous studies, is summarized in Table S4. Hygroscopic growth of inhaled particles occurs over time scales ranging from milliseconds to

https://doi.org/10.1021/acs.est.4c08315
Environ. Sci. Technol. XXXX, XXX, XXX−XXX

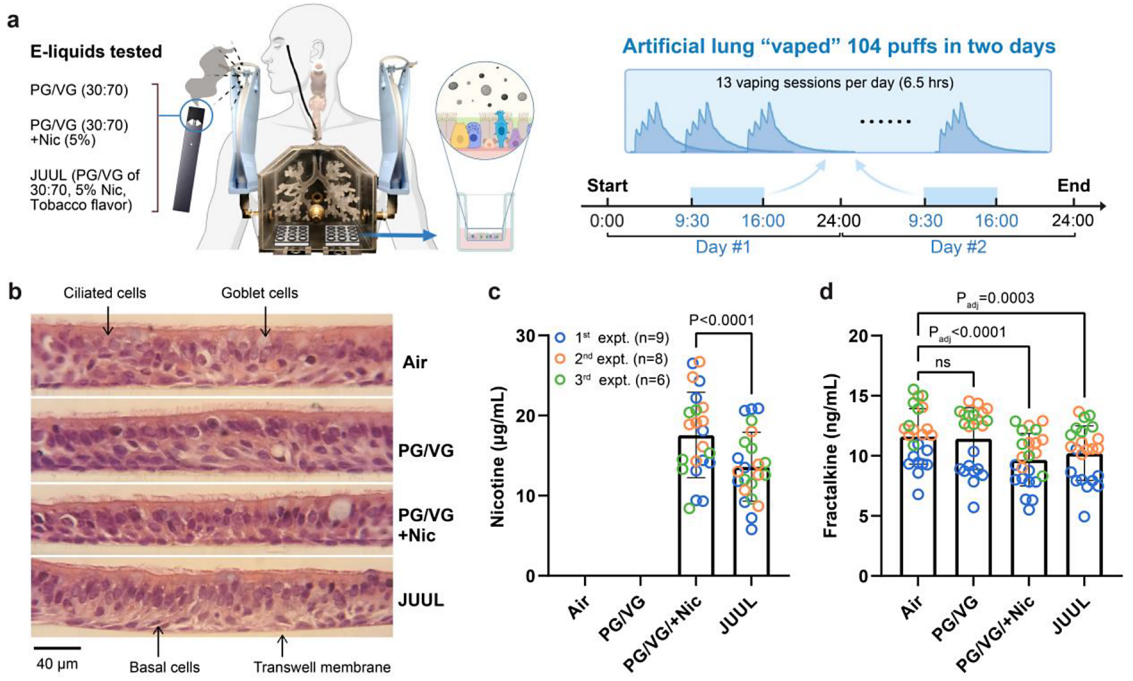

Figure 5. Impact of e-cig aerosol exposure on airway epithelium from simulated vaping scenarios. (a) Schematic illustration of human bronchial epithelial cells (HBECs) exposed to e-cig aerosols within the artificial lung over 2 days. Primary HBECs from a healthy nonsmoking donor were cultured under air−liquid interface (ALI) conditions and fully differentiated into pseudostratified mucociliary epithelium. Replicate ALI cultures of HBECs were exposed to clean air (control group) or different e-cig aerosols (experimental group) for 2 days, using a vaping regimen of 4 puffs per 30 min session (Figure 1c), 13 sessions per day, totaling 104 puffs. The tested e-cig aerosols were produced using a JUUL device filled with either lab-made e-liquids [propylene glycol/vegetable glycerin (PG/VG) in a 30:70 ratio, with or without 5% nicotine benzoate] or marketed JUUL Virginia Tobacco pods (containing 5% nicotine benzoate). Three independent experiments were conducted with sample sizes of n = 9, 8, and 6 for each group, respectively, each using different batches of ALI cultures of HBECs from the same donor at the same passage. (b) Representative ALI cultures of HBECs from each group after the two-day exposure were prepared for histological analysis, stained with hematoxylin and eosin (H&E) and imaged at 20× magnification. (c) Nicotine levels in the HBEC culture supernatant after the two-day exposure (total n = 23 for each group, with samples from each experiment indicated with different colored dots). Differences in nicotine levels between the PG/VG+Nic and JUUL groups were tested using a paired t test, matching the well locations in the plate. (d) Chemokine Fractalkine (CX3CL1) levels in the HBEC culture supernatant after the two-day exposure (total n = 23 for each group, with samples from each experiment indicated with different colored dots). Differences in Fractalkine levels among the four groups were tested using ANOVA with multiple comparisons. Adjusted p-values from comparing each exposure group to the control group are shown in the figure.

seconds or longer, which aligns with breathing cycles.[62,63] Consequently, this growth substantially impacts particle deposition in the lungs.[64−66] By replicating the lung environment, our artificial lung system could characterize aerosol dynamics as they occur in human lungs, providing more human-relevant data for assessing exposure risks and determining administrative doses of various aerosols.

3.4. Proof-of-Concept Study on Toxicological Effects of E-cig Aerosol. Our artificial lung system replicates several key aspects of human inhalation exposure and therefore facilitates inhalation toxicology studies with greater physiological relevance than traditional methods. As a proof of principle, we exposed cultured human primary bronchial epithelium to e-cig aerosols generated from different e-liquids formulations using a simulated vaping scenario over 2 days (Figure 5a and Methods). The e-cig aerosols produced from these three e-liquids exhibited similar, but not identical, trimodal size distributions (Figure S6a). Specifically, the PG/VG, PG/VG+Nic, and marketed JUUL Virginia Tobacco pods, featured increased levels of micron (>1 μm), submicron (100−1000 nm), and ultrafine particles (<100 nm), respectively. Consequently, the JUUL Virginia Tobacco pods, which contained a complete set of e-liquid constituents had the greatest number of particles, but the least aerosol mass compared to e-liquids with partial constituents (Figure S6b).

HBECs cultured under ALI conditions differentiated into a pseudostratified mucociliary epithelium in each well, comprising various airway epithelial cells, including goblet cells, ciliated cells, and basal cells (Figure 5b). After exposure to e-cig aerosols, the pseudostratified mucociliary epithelium in each group maintained its cellular structures with no observed histological changes. Nicotine levels in the cell culture supernatant after exposure confirmed nicotine delivery to the airway epithelium from both the lab-made e-liquid (PG/VG+Nic) and the marketed JUUL pods (Figure 5c). The different nicotine doses received by the two groups were likely due to variations in e-liquid composition (e.g., flavor and other additives) affecting the emission of nicotine-containing aerosols. As suggested by aerosol characterization results (Figure S6), the marketed JUUL pods yielded less aerosol mass than the lab-made e-liquid (PG/VG+Nic). Despite these slight differences, exposure to both nicotine-containing aerosols (PG/VG+Nic and JUUL) resulted in decreased levels of chemokine Fractalkine (CX3CL1) released by HBECs into the culture supernatant (Figure 5d). Fractalkine is an important regulator of immune cells involved in inflammatory responses to inhaled toxicants. Our results align with human studies showing lower levels of Fractalkine in the

https://doi.org/10.1021/acs.est.4c08315
Environ. Sci. Technol. XXXX, XXX, XXX−XXX

airways of healthy e-cig users compared to nonusers, along with other biomarkers suggesting overall suppressed immune responses due to e-cig use.[67,68] The observed decrease in Fractalkine in response to e-cig aerosol exposure is likely due to the effects of nicotine.

3.5. Innovation, Limitations, and Future Directions. Studying aerosol exposures in human lungs and associated biological effects is crucial for understanding their health risks and developing mitigation and treatment strategies for related diseases. However, current inhalation toxicology methods often fail to replicate the dynamic interactions between inhaled aerosols and the respiratory system.[17−22] Our developed artificial lung system includes continuous breathing, transitional airflow fields in 3D-printed airways, and the warm and humid lung environment. This system therefore replicates key aspects of human inhalation exposure including gradual clearance, size-dependent deposition, and aerosol dynamics, as occurs in real human lungs. When combined with ALI cultures of HBECs, our artificial lung system provides a more physiologically relevant in vitro exposure model for studying respiratory toxicology and pharmacology. As demonstrated in this study, short-term exposure to e-cig aerosols from simulated vaping for 2 days altered epithelial production of Fractalkine, an established mediator of inflammation and immune responses related to chronic obstructive pulmonary disease (COPD).[69] In comparison, our prior studies employing traditional in vitro (cell lines) and in vivo (mice) approaches demonstrated acute toxic effects, including cell death and lung injuries resulting from even fewer vaping puffs (5−120 puffs).[53,70] This difference highlights the limitations of conventional toxicology approaches, which use simplified exposure protocols and lack human physiological relevance. Although our current study on e-cig aerosols focused on specific toxicological assessments as a proof of principle to demonstrate the functionality of the artificial lung system, the cultured HBECs, which preserve the cellular structures and biological functions of the native airway epithelium, will also facilitate studies on exposure-induced biochemical reactions and provide additional insights into mechanisms of inhalation toxicity. Additionally, long-term exposure can be achieved in the future since the cultured HBECs can generate a self-sustaining epithelial layer for several months. In summary, the artificial lung system holds the potential for wider application in various inhalation exposure studies, especially in evaluating and comparing the inhalation toxicity of different tobacco products, thus informing regulatory decision-making. The uniqueness of our artificial lung system in facilitating physiologically relevant inhalation exposure studies compared to traditional toxicology models are summarized in Table S5.

It must be noted that the current artificial lung system has several limitations. Although the elastic lung balloons accommodate volume changes during respiration and drive symmetric airflow patterns, the rigid lung chamber itself cannot expand and contract as real human lungs. Currently, the system focuses on simulating vaping exposure using an upper airway model with a mouth tract to replicate mouth-breathing. In the future, it can be adapted to include a nasal tract for studying the inhalation exposure and health effects of other emerging environmental aerosols, such as wildfire smoke, brake and tire wear particles, and airborne microplastics.[71] The current airway replica spans only from the mouth inlet to airway G13, primarily due to the resolution limits when 3D printing the geometrically complex airway structures. Despite this, the model effectively recreates the regional airflow fields and fractionally deposits inhaled particles, thus exposing the bronchial epithelium to the aerosol fraction that would reach the bronchus under their characteristic laminar airflow conditions. While the current model is a valuable tool for studying exposures in the conducting airways, further development is underway to include alveolar exposures. This will involve constructing porous microhoneycomb structures to achieve expansive surface areas and near-diffusion airflow, characteristic of the alveolar compartment.[72] Consequently, the air-blood barrier cocultures will replace HBEC cultures for biological and toxicological assessments. Furthermore, individualized lung models can be developed with variable lung volumes and airway geometries, along with specific respiratory parameters and cellular biology, to account for differences across diverse demographic groups (e.g., age, sex, and ethnicity) and health conditions (e.g., healthy individuals and those with obstructive lung diseases). This capability of the artificial lung system enables precise exposure risk assessments, providing novel insights into individual susceptibility to inhalation exposures and lung toxicity.

■ ASSOCIATED CONTENT

Supporting Information

The Supporting Information is available free of charge at https://pubs.acs.org/doi/10.1021/acs.est.4c08315.

Materials and methods for developing the artificial lung system; methods of conducting computational fluid-particle dynamics (CFPD) simulations; materials and methods for the cultivation of primary human bronchial epithelial cells (HBECs); calculation of the particle decay rate and deposition in the 3D-printed airways; schematic experimental setup for characterizing DEHS and NaCl particles; size-distributions of the generated DEHS and NaCl particles; the experimental setting for exposing human primary bronchial epithelial cells (HBECs) to e-cigarette aerosols from realistic vaping scenarios; airflow velocity distributions in the airway structures at different time points over a full respiratory cycle; transport dynamics and deposition of particles of different sizes within airway structures at different time points during inhalation; the characteristics of e-cigarette aerosols generated using different e-liquids; the basic modeling parameters for the MPPD model prediction; the observed bimodal size characteristics of e-cig particles under different environments used for the estimation of the deposition fractions; reference density of particles tested in this study; the hygroscopic growth factors of various aerosol particles from the literature; the comparison of the artificial lung system with conventional in vitro/in vivo toxicology approaches for studying human inhalation exposure; and additional references (PDF)

Visualization of the distribution of inhaled aerosols through 3D-printed airway structures (MP4)

Visualization of the impact of lung environments on inhaled e-cig aerosols (MP4)

■ AUTHOR INFORMATION

Corresponding Author

Yifang Zhu − *Department of Environmental Health Sciences, Jonathan and Karin Fielding School of Public Health, University of California, Los Angeles, California 90095, United States;* orcid.org/0000-0002-0591-3322; Email: yifang@ucla.edu

https://doi.org/10.1021/acs.est.4c08315
Environ. Sci. Technol. XXXX, XXX, XXX−XXX

Authors

Haoxuan Chen − *Department of Environmental Health Sciences, Jonathan and Karin Fielding School of Public Health, University of California, Los Angeles, California 90095, United States;* orcid.org/0000-0001-8398-9093

Airi Harui − *Division of Pulmonary and Critical Care, Department of Medicine, David Geffen School of Medicine, University of California, Los Angeles, California 90095, United States*

Yu Feng − *School of Chemical Engineering, Oklahoma State University, Stillwater, Oklahoma 74078, United States*

Liqiao Li − *Department of Environmental Health Sciences, Jonathan and Karin Fielding School of Public Health, University of California, Los Angeles, California 90095, United States;* orcid.org/0000-0002-8873-1275

Saagar Patel − *Institute of the Environment and Sustainability, University of California, Los Angeles, California 90095, United States*

Jacob Schmidt − *Department of Bioengineering, Samueli School of Engineering, University of California, Los Angeles, California 90095, United States*

Michael D. Roth − *Division of Pulmonary and Critical Care, Department of Medicine, David Geffen School of Medicine, University of California, Los Angeles, California 90095, United States*

Complete contact information is available at: https://pubs.acs.org/10.1021/acs.est.4c08315

Notes

The authors declare no competing financial interest.

■ ACKNOWLEDGMENTS

This study is supported by the National Institutes of Health (grant NHLBI R01 HL139379 (Y. Zhu)), the California Bureau of Cannabis Control (grant 65309 (M.D. Roth)), and the Tobacco-Related Disease Research Program (grant T33FT6351 (H. Chen)). The TOC graphic was created with BioRender.com.

■ REFERENCES

(1) Keswani, A.; Akselrod, H.; Anenberg, S. C. Health and clinical impacts of air pollution and linkages with climate change. *NEJM Evidence* **2022**, *1* (7), No. EVIDra2200068.

(2) Wang, C. C.; Prather, K. A.; Sznitman, J.; Jimenez, J. L.; Lakdawala, S. S.; Tufekci, Z.; Marr, L. C. Airborne transmission of respiratory viruses. *Science* **2021**, *373* (6558), No. eabd9149.

(3) Dinakar, C.; O'Connor, G. T. The health effects of electronic cigarettes. *N. Engl. J. Med.* **2016**, *375* (14), 1372−1381.

(4) Sridharan, S.; Kumar, M.; Singh, L.; Bolan, N. S.; Saha, M. Microplastics as an emerging source of particulate air pollution: A critical review. *J. Hazard. Mater.* **2021**, *418*, No. 126245.

(5) Patel, G.; Patra, C.; Srinivas, S. P.; Kumawat, M.; Navya, P. N.; Daima, H. K. Methods to evaluate the toxicity of engineered nanomaterials for biomedical applications: A review. *Environ. Chem. Lett.* **2021**, *19* (6), 4253−4274.

(6) Li, T.; Yu, Y.; Sun, Z.; Duan, J. A comprehensive understanding of ambient particulate matter and its components on the adverse health effects based from epidemiological and laboratory evidence. *Part. Fibre Toxicol.* **2022**, *19* (1), 67.

(7) World Health Organization *Global health estimates: Life expectancy and leading causes of death and disability*, 2024. https://www.who.int/data/gho/data/themes/mortality-and-global-health-estimates (accessed 2024 Nov-7).

(8) *Institute for Health Metrics and Evaluation (IHME), GBD Results*. IHME, University of Washington: Seattle, WA, 2024. https://vizhub.healthdata.org/gbd-results (accessed 2024 Nov-7).

(9) Health Effects Institute *State of global air 2024*; Health Effects Institute: Boston, MA, 2024. https://www.stateofglobalair.org/resources/report/state-global-air-report-2024.

(10) Movia, D.; Bruni-Favier, S.; Prina-Mello, A. In vitro alternatives to acute inhalation toxicity studies in animal models—a perspective. *Front. Bioeng. Biotechnol.* **2020**, *8*, 549.

(11) Yang, S.; Chen, Z.; Cheng, Y.; Liu, T.; Lihong, Y.; Pu, Y.; Liang, G. Environmental toxicology wars: Organ-on-a-chip for assessing the toxicity of environmental pollutants. *Environ. Pollut.* **2021**, *268*, No. 115861.

(12) U.S. EPA. *Guidelines for Exposure Assessment (1992)*. U.S. Environmental Protection Agency, Risk Assessment Forum: Washington, DC, EPA/600/Z-92/001, 1992.

(13) Hinds, W. C.; Zhu, Y. *Aerosol Technology: Properties, Behavior, and Measurement of Airborne Particles*; John Wiley & Sons, 2022.

(14) Carvalho, T. C.; Peters, J. I.; Williams, R. O. Influence of particle size on regional lung deposition−what evidence is there? *Int. J. Pharm.* **2011**, *406* (1−2), 1−10.

(15) Yeh, H.; Phalen, R.; Raabe, O. Factors influencing the deposition of inhaled particles. *Environ. Health Perspect.* **1976**, *15*, 147−156.

(16) ICRP. Human respiratory tract model for radiological protection. A report of a task group of the international commission on radiological protection. *Ann. ICRP* **1994**, *24* (1−3), 1−482.

(17) Yue, Y.; Chen, H.; Setyan, A.; Elser, M.; Dietrich, M.; Li, J.; Zhang, T.; Zhang, X.; Zheng, Y.; Wang, J.; Yao, M. Size-resolved endotoxin and oxidative potential of ambient particles in beijing and zürich. *Environ. Sci. Technol.* **2018**, *52* (12), 6816−6824.

(18) Hammer, T.; Gao, H.; Pan, Z.; Wang, J. Relationship between aerosols exposure and lung deposition dose. *Aerosol Air Qual. Res.* **2020**, *20* (5), 1083−1093.

(19) Madureira, J.; Slezakova, K.; Silva, A. I.; Lage, B.; Mendes, A.; Aguiar, L.; Pereira, M. C.; Teixeira, J. P.; Costa, C. Assessment of indoor air exposure at residential homes: Inhalation dose and lung deposition of pm10, pm2.5 and ultrafine particles among newborn children and their mothers. *Sci. Total Environ.* **2020**, *717*, No. 137293.

(20) Secondo, L. E.; Sagona, J. A.; Calderón, L.; Wang, Z.; Plotnik, D.; Senick, J.; Sorensen-Allacci, M.; Wener, R.; Andrews, C. J.; Mainelis, G. Estimating lung deposition of fungal spores using actual airborne spore concentrations and physiological data. *Environ. Sci. Technol.* **2021**, *55* (3), 1852−1863.

(21) Patel, S.; Sankhyan, S.; Boedicker, E. K.; DeCarlo, P. F.; Farmer, D. K.; Goldstein, A. H.; Katz, E. F.; Nazaroff, W. W.; Tian, Y.; Vanhanen, J.; Vance, M. E. Indoor particulate matter during homechem: Concentrations, size distributions, and exposures. *Environ. Sci. Technol.* **2020**, *54* (12), 7107−7116.

(22) Son, Y.; Mainelis, G.; Delnevo, C.; Wackowski, O. A.; Schwander, S.; Meng, Q. Investigating e-cigarette particle emissions and human airway depositions under various e-cigarette-use conditions. *Chem. Res. Toxicol.* **2020**, *33* (2), 343−352.

(23) Sosnowski, T. R.; Odziomek, M. Particle size dynamics: Toward a better understanding of electronic cigarette aerosol interactions with the respiratory system. *Front. Physiol.* **2018**, *9*, 853.

(24) Pichelstorfer, L.; Hofmann, W.; Winkler-Heil, R.; Yurteri, C. U.; McAughey, J. Simulation of aerosol dynamics and deposition of combustible and electronic cigarette aerosols in the human respiratory tract. *J. Aerosol Sci.* **2016**, *99*, 125−132.

(25) Feng, Y.; Kleinstreuer, C.; Rostami, A. Evaporation and condensation of multicomponent electronic cigarette droplets and conventional cigarette smoke particles in an idealized g3−g6 triple bifurcating unit. *J. Aerosol Sci.* **2015**, *80*, 58−74.

(26) Singh, A. V.; Ansari, M. H. D.; Rosenkranz, D.; Maharjan, R. S.; Kriegel, F. L.; Gandhi, K.; Kanase, A.; Singh, R.; Laux, P.; Luch, A. Artificial intelligence and machine learning in computational nanotoxicology: Unlocking and empowering nanomedicine. *Adv. Healthcare Mater.* **2020**, *9* (17), No. 1901862.

https://doi.org/10.1021/acs.est.4c08315
Environ. Sci. Technol. XXXX, XXX, XXX−XXX

(27) Singh, A. V.; Varma, M.; Rai, M.; Pratap Singh, S.; Bansod, G.; Laux, P.; Luch, A. Advancing predictive risk assessment of chemicals via integrating machine learning, computational modeling, and chemical/nano-quantitative structure-activity relationship approaches. *Adv. Intell. Syst.* **2024**, *6* (4), No. 2300366.
(28) Hofmann, W. Modelling particle deposition in human lungs: Modelling concepts and comparison with experimental data. *Biomarkers* **2009**, *14* (sup1), 59−62.
(29) Lim, S. H.; Park, S.; Lee, C. C.; Ho, P. C. L.; Kwok, P. C. L.; Kang, L. A 3d printed human upper respiratory tract model for particulate deposition profiling. *Int. J. Pharm.* **2021**, *597*, No. 120307.
(30) Kolewe, E. L.; Feng, Y.; Fromen, C. A. Realizing lobe-specific aerosol targeting in a 3d-printed in vitro lung model. *J. Aerosol Med. Pulm. Drug Delivery* **2021**, *34* (1), 42−56.
(31) Su, W.-C.; Chen, Y.; Xi, J. A new approach to estimate ultrafine particle respiratory deposition. *Inhalation Toxicol.* **2019**, *31* (1), 35−43.
(32) Singh, A. V.; Romeo, A.; Scott, K.; Wagener, S.; Leibrock, L.; Laux, P.; Luch, A.; Kerkar, P.; Balakrishnan, S.; Dakua, S. P.; Park, B.-W. Emerging technologies for in vitro inhalation toxicology. *Adv. Healthcare Mater.* **2021**, *10* (18), No. 2100633.
(33) Singh, A. V.; Maharjan, R. S.; Kromer, C.; Laux, P.; Luch, A.; Vats, T.; Chandrasekar, V.; Dakua, S. P.; Park, B.-W. Advances in smoking related in vitro inhalation toxicology: A perspective case of challenges and opportunities from progresses in lung-on-chip technologies. *Chem. Res. Toxicol.* **2021**, *34* (9), 1984−2002.
(34) Clippinger, A. J.; Allen, D.; Jarabek, A. M.; Corvaro, M.; Gaça, M.; Gehen, S.; Hotchkiss, J. A.; Patlewicz, G.; Melbourne, J.; Hinderliter, P.; Yoon, M.; Huh, D.; Lowit, A.; Buckley, B.; Bartels, M.; BéruBé, K.; Wilson, D. M.; Indans, I.; Vinken, M. Alternative approaches for acute inhalation toxicity testing to address global regulatory and non-regulatory data requirements: An international workshop report. *Toxicol. In Vitro* **2018**, *48*, 53−70.
(35) Cao, X.; Coyle, J. P.; Xiong, R.; Wang, Y.; Heflich, R. H.; Ren, B.; Gwinn, W. M.; Hayden, P.; Rojanasakul, L. Invited review: Human air-liquid-interface organotypic airway tissue models derived from primary tracheobronchial epithelial cells—overview and perspectives. *In Vitro Cell. Dev. Biol. Anim.* **2021**, *57* (2), 104−132.
(36) Lacroix, G.; Koch, W.; Ritter, D.; Gutleb, A. C.; Larsen, S. T.; Loret, T.; Zanetti, F.; Constant, S.; Chortarea, S.; Rothen-Rutishauser, B.; Hiemstra, P. S.; Frejafon, E.; Hubert, P.; Gribaldo, L.; Kearns, P.; Aublant, J.-M.; Diabaté, S.; Weiss, C.; de Groot, A.; Kooter, I. Air−liquid interface in vitro models for respiratory toxicology research: Consensus workshop and recommendations. *Appl. In Vitro Toxicol.* **2018**, *4* (2), 91−106.
(37) Leni, Z.; Ess, M. N.; Keller, A.; Allan, J. D.; Hellén, H.; Saarnio, K.; Williams, K. R.; Brown, A. S.; Salathe, M.; Baumlin, N.; Vasilatou, K.; Geiser, M. Role of secondary organic matter on soot particle toxicity in reconstituted human bronchial epithelia exposed at the air−liquid interface. *Environ. Sci. Technol.* **2022**, *56* (23), 17007−17017.
(38) Lee, M. K. H.; Lim, H. K.; Su, C.; Koh, J. Y. C.; Setyawati, M. I.; Ng, K. W.; Hou, H. W.; Tay, C. Y. 3d airway epithelial−fibroblast biomimetic microfluidic platform to unravel engineered nanoparticle-induced acute stress responses as exposome determinants. *Environ. Sci. Technol.* **2023**, *57* (48), 19223−19235.
(39) Benam, K. H.; Villenave, R.; Lucchesi, C.; Varone, A.; Hubeau, C.; Lee, H.-H.; Alves, S. E.; Salmon, M.; Ferrante, T. C.; Weaver, J. C.; Bahinski, A.; Hamilton, G. A.; Ingber, D. E. Small airway-on-a-chip enables analysis of human lung inflammation and drug responses in vitro. *Nat. Methods* **2016**, *13* (2), 151−157.
(40) Benam, K. H.; Novak, R.; Ferrante, T. C.; Choe, Y.; Ingber, D. E. Biomimetic smoking robot for in vitro inhalation exposure compatible with microfluidic organ chips. *Nat. Protoc.* **2020**, *15* (2), 183−206.
(41) Bai, H.; Si, L.; Jiang, A.; Belgur, C.; Zhai, Y.; Plebani, R.; Oh, C. Y.; Rodas, M.; Patil, A.; Nurani, A.; Gilpin, S. E.; Powers, R. K.; Goyal, G.; Prantil-Baun, R.; Ingber, D. E. Mechanical control of innate immune responses against viral infection revealed in a human lung alveolus chip. *Nat. Commun.* **2022**, *13* (1), 1928.
(42) Liu, C.; Hu, H.; Zhou, S.; Chen, X.; Hu, Y.; Hu, J. Change of composition, source contribution, and oxidative effects of environmental pm2.5 in the respiratory tract. *Environ. Sci. Technol.* **2023**, *57* (31), 11605−11611.
(43) LeMessurier, K. S.; Tiwary, M.; Morin, N. P.; Samarasinghe, A. E. Respiratory barrier as a safeguard and regulator of defense against influenza a virus and streptococcus pneumoniae. *Front. Immunol.* **2020**, *11*, DOI: .
(44) Neczypor, E. W.; Mears, M. J.; Ghosh, A.; Sassano, M. F.; Gumina, R. J.; Wold, L. E.; Tarran, R. E-cigarettes and cardiopulmonary health: Review for clinicians. *Circulation* **2022**, *145* (3), 219−232.
(45) Wold, L. E.; Tarran, R.; Crotty Alexander, L. E.; Hamburg, N. M.; Kheradmand, F.; St. Helen, G.; Wu, J. C. Cardiopulmonary consequences of vaping in adolescents: A scientific statement from the American heart association. *Circ. Res.* **2022**, *131* (3), e70−e82.
(46) Forest, V.; Mercier, C.; Pourchez, J. Considerations on dosimetry for in vitro assessment of e-cigarette toxicity. *Respir. Res.* **2022**, *23* (1), 358.
(47) Spahn, J. E.; Stavchansky, S. A.; Cui, Z. Critical research gaps in electronic cigarette devices and nicotine aerosols. *Int. J. Pharm.* **2021**, *593*, No. 120144.
(48) Stanojevic, S.; Graham, B. L.; Cooper, B. G.; Thompson, B. R.; Carter, K. W.; Francis, R. W.; Hall, G. L. Official ers technical standards: Global lung function initiative reference values for the carbon monoxide transfer factor for caucasians. *Eur. Respir. J.* **2017**, *50* (3), 1700010.
(49) Kitaoka, H.; Koc, S.; Tetsumoto, S.; Koumo, S.; Hirata, H.; Kijima, T.; *4d model generator of the human lung, lung4cer*. In Annual International Conference of the IEEE Engineering in Medicine and Biology Society (EMBC), 2013.
(50) Hayati, H.; Feng, Y.; Hinsdale, M. Inter-species variabilities of droplet transport, size change, and deposition in human and rat respiratory systems: An in silico study. *J. Aerosol Sci.* **2021**, *154*, No. 105761.
(51) Zarei, S.; Mirtar, A.; Andresen, B.; Salamon, P. Modeling the airflow in a lung with cystic fibrosis. *J. Non-Equilib. Thermodyn.* **2013**, *38* (2), 119−140.
(52) Li, L.; Lee, E. S.; Nguyen, C.; Zhu, Y. Effects of propylene glycol, vegetable glycerin, and nicotine on emissions and dynamics of electronic cigarette aerosols. *Aerosol Sci. Technol.* **2020**, *54* (11), 1270−1281.
(53) Ma, T.; Chen, H.; Liao, Y.-P.; Li, J.; Wang, X.; Li, L.; Li, J.; Zhu, Y.; Xia, T. Differential toxicity of electronic cigarette aerosols generated from different generations of devices in vitro and in vivo. *Environ. Health* **2023**, *1* (5), 315−323.
(54) Belsare, P.; Senyurek, V. Y.; Imtiaz, M. H.; Tiffany, S.; Sazonov, E. Computation of cigarette smoke exposure metrics from breathing. *IEEE Trans. Biomed. Eng.* **2020**, *67* (8), 2309−2316.
(55) Miller, F. J.; Asgharian, B.; Schroeter, J. D.; Price, O. Improvements and additions to the multiple path particle dosimetry model. *J. Aerosol Sci.* **2016**, *99*, 14−26.
(56) Hiemstra, P. S.; Grootaers, G.; van der Does, A. M.; Krul, C. A. M.; Kooter, I. M. Human lung epithelial cell cultures for analysis of inhaled toxicants: Lessons learned and future directions. *Toxicol. In Vitro* **2018**, *47*, 137−146.
(57) Ali, F. R. M.; Seaman, E. L.; Crane, E.; Schillo, B.; King, B. A. Trends in us e-cigarette sales and prices by nicotine strength, overall and by product and flavor type, 2017−2022. *Nicotine Tobacco Res.* **2023**, *25* (5), 1052−1056.
(58) Li, L.; Nguyen, C.; Lin, Y.; Guo, Y.; Fadel, N. A.; Zhu, Y. Impacts of electronic cigarettes usage on air quality of vape shops and their nearby areas. *Sci. Total Environ.* **2021**, *760*, No. 143423.
(59) Stahlhofen, W.; Rudolf, G.; James, A. C. Intercomparison of experimental regional aerosol deposition data. *J. Aerosol Med.* **1989**, *2* (3), 285−308.
(60) Balásházy, I.; Hofmann, W.; Heistracher, T. Local particle deposition patterns may play a key role in the development of lung cancer. *J. Appl. Physiol.* **2003**, *94* (5), 1719−1725.
(61) Hofmann, W. Modelling inhaled particle deposition in the human lung—a review. *J. Aerosol Sci.* **2011**, *42* (10), 693−724.

https://doi.org/10.1021/acs.est.4c08315
Environ. Sci. Technol. XXXX, XXX, XXX−XXX

(62) Denjean, C. *Aerosol Hygroscopicity*. In Atmospheric Chemistry in the Mediterranean Region: Vol. 2—From Air Pollutant Sources to Impacts, Dulac, F.; Sauvage, S.; Hamonou, E., Eds.; Springer International Publishing, 2022; pp 285−301.
(63) Haddrell, A. E.; Lewis, D.; Church, T.; Vehring, R.; Murnane, D.; Reid, J. P. Pulmonary aerosol delivery and the importance of growth dynamics. *Ther. Delivery* **2017**, *8* (12), 1051−1061.
(64) Farkas, Á.; Füri, P.; Thén, W.; Salma, I. Effects of hygroscopic growth of ambient urban aerosol particles on their modelled regional and local deposition in healthy and copd-compromised human respiratory system. *Sci. Total Environ.* **2022**, *806*, No. 151202.
(65) Man, R.; Wu, Z.; Zong, T.; Voliotis, A.; Qiu, Y.; Größ, J.; van Pinxteren, D.; Zeng, L.; Herrmann, H.; Wiedensohler, A.; Hu, M. Impact of water uptake and mixing state on submicron particle deposition in the human respiratory tract (hrt) based on explicit hygroscopicity measurements at hrt-like conditions. *Atmos. Chem. Phys.* **2022**, *22* (18), 12387−12399.
(66) Ching, J.; Kajino, M.; Matsui, H. Resolving aerosol mixing state increases accuracy of black carbon respiratory deposition estimates. *One Earth* **2020**, *3* (6), 763−776.
(67) Sayed, I. M.; Masso-Silva, J. A.; Mittal, A.; Patel, A.; Lin, E.; Moshensky, A.; Shin, J.; Bojanowski, C. M.; Das, S.; Akuthota, P.; Crotty Alexander, L. E. Inflammatory phenotype modulation in the respiratory tract and systemic circulation of e-cigarette users: A pilot study. *Am. J. Physiol. Lung Cell Mol. Physiol.* **2021**, *321* (6), L1134−l1146.
(68) Martin, E. M.; Clapp, P. W.; Rebuli, M. E.; Pawlak, E. A.; Glista-Baker, E.; Benowitz, N. L.; Fry, R. C.; Jaspers, I. E-cigarette use results in suppression of immune and inflammatory-response genes in nasal epithelial cells similar to cigarette smoke. *Am. J. Physiol. Lung Cell Mol. Physiol.* **2016**, *311* (1), L135−144.
(69) McComb, J. G.; Ranganathan, M.; Liu, X. H.; Pilewski, J. M.; Ray, P.; Watkins, S. C.; Choi, A. M. K.; Lee, J. S. Cx3cl1 up-regulation is associated with recruitment of CX3cr1+ mononuclear phagocytes and t lymphocytes in the lungs during cigarette smoke-induced emphysema. *Am. J. Pathol.* **2008**, *173* (4), 949−961.
(70) Ma, T.; Wang, X.; Li, L.; Sun, B.; Zhu, Y.; Xia, T. Electronic cigarette aerosols induce oxidative stress-dependent cell death and NF-κB mediated acute lung inflammation in mice. *Arch. Toxicol.* **2021**, *95* (1), 195−205.
(71) Rosati Rowe, J. A.; Burton, R.; McGregor, G.; McCauley, R.; Tang, W.; Spencer, R. Development of a three-dimensional model of the human respiratory system for dosimetric use. *Theor. Biol. Med. Modell.* **2013**, *10* (1), 28.
(72) Sznitman, J. Revisiting airflow and aerosol transport phenomena in the deep lungs with microfluidics. *Chem. Rev.* **2022**, *122* (7), 7182−7204.

https://doi.org/10.1021/acs.est.4c08315
Environ. Sci. Technol. XXXX, XXX, XXX−XXX